Smart Structures and Systems, *Vol. 30, No. 5 (2022) 521-535*
https://doi.org/10.12989/sss.2022.30.5.521

Computer vision-based remote displacement monitoring system for in-situ bridge bearings robust to large displacement induced by temperature change

Byunghyun Kim [1], Junhwa Lee [2], Sung-Han Sim [3], Soojin Cho*[1] and Byung Ho Park [4]

[1] *Department of Civil Engineering, University of Seoul, 163 Seoulsiripdae-ro, Dongdaemun-gu, Seoul 02504, Republic of Korea*
[2] *Department of Urban and Environmental Engineering, Ulsan National Institute of Science and Technology (UNIST), 50 UNIST-gil, Ulju-gun, Ulsan 44919, Republic of Korea*
[3] *School of Civil, Architectural Engineering and Landscape Architecture, Sungkyunkwan University, 2066 Seoburo, Jangan-gu, Suwon 16419, Republic of Korea*
[4] *Technology Innovation Center, Seoul Facilities Corporation, 527-6 Majang-dong, Seongdong-gu, Seoul 04704, Republic of Korea*

(*Received November 10, 2021, Revised September 21, 2022, Accepted October 27, 2022*)

Abstract. Efficient management of deteriorating civil infrastructure is one of the most important research topics in many developed countries. In particular, the remote displacement measurement of bridges using linear variable differential transformers, global positioning systems, laser Doppler vibrometers, and computer vision technologies has been attempted extensively. This paper proposes a remote displacement measurement system using closed-circuit televisions (CCTVs) and a computer-vision-based method for in-situ bridge bearings having relatively large displacement due to temperature change in long term. The hardware of the system is composed of a reference target for displacement measurement, a CCTV to capture target images, a gateway to transmit images via a mobile network, and a central server to store and process transmitted images. The usage of CCTV capable of night vision capture and wireless data communication enable long-term 24-hour monitoring on wide range of bridge area. The computer vision algorithm to estimate displacement from the images involves image preprocessing for enhancing the circular features of the target, circular Hough transformation for detecting circles on the target in the whole field-of-view (FOV), and homography transformation for converting the movement of the target in the images into an actual expansion displacement. The simple target design and robust circle detection algorithm help to measure displacement using target images where the targets are far apart from each other. The proposed system is installed at the Tancheon Overpass located in Seoul, and field experiments are performed to evaluate the accuracy of circle detection and displacement measurements. The circle detection accuracy is evaluated using 28,542 images captured from 71 CCTVs installed at the testbed, and only 48 images (0.168%) fail to detect the circles on the target because of subpar imaging conditions. The accuracy of displacement measurement is evaluated using images captured for 17 days from three CCTVs; the average and root-mean-square errors are 0.10 and 0.131 mm, respectively, compared with a similar displacement measurement. The long-term operation of the system, as evaluated using 8-month data, shows high accuracy and stability of the proposed system.

Keywords: bridge expansion displacement; circular hough transformation; closed-circuit televisions; computer vision-based displacement measurement; homography transformation

1. Introduction

The increasing number of deteriorating structures and their maintenance are typical public issues in many well-developed countries. In South Korea, the proportion of bridges older than 30 years is estimated to be 13.7% as of 2020 but it will reach 42.2% by2030 (Park and Lee 2016). Bridge bearings are one of the most important components of bridges because they deliver dead and live loads vertically to piers while evading horizontal earthquakes and temperature loads. During service, the horizontal displacement of the bridge bearings can be measured to evaluate their capability. In South Korea, the infrastructure inspection guideline (Korean Authority of Land and Infrastructure Safety 2019) designates the regular publication of reports regarding the external damage of bridge bearings, as well as the shortage of thermal expansion displacement. In the United States, bridge bearings must be designed to facilitate the horizontal displacement of superstructures due to temperature changes (Federal Highway Administration 2007). The anomaly of expansion displacement should be managed accordingly because it may cause severe damage to the structure. Restricting main girder movements may harm girders or slabs under abrupt temperature increases, whereas excessive expansive displacements can damage the superstructure and expansion joints. Damage to expansion joints may cause road undulations nearby, which can exacerbate the vehicle impact load and cause car accidents on the bridge.

The horizontal displacement of a bridge bearing is an important indicator of the structural health of a bridge; however, assessing the bridge bearing daily or weekly to measure the horizontal displacement is insufficient. Hence, a displacement measurement system must be developed for

*Corresponding author, Professor,
E-mail: soojin@uos.ac.kr

ISSN: 1738-1584 (Print), 1738-1991 (Online)

bridge-bearing monitoring. To develop a widely applicable and practical bridge bearing displacement measurement system, the following requirements must be fulfilled.

1. The system should be cost-effective and easy to install on multiple piers in a facile manner.
2. The system should measure displacement in a non-contact manner to avoid sensor damage due to bridge bearing damage or movement.
3. The system should be able to measure relatively large displacements up to tens of millimeters, which is the span of typical bridge bearings, while maintaining a small resolution in the order of submillimeters. The system should not require a high sampling frequency because the bearing displacement is primarily affected by long-term static loads (e.g., temperature loads).
4. The system should be able to measure displacements stably under various outdoor imaging conditions, e.g., rain, dirt, and intense sunlight.

In recent years, many studies have been conducted regarding the displacement measurement of bridge bearings using contact-type sensors. For instance, Guo *et al*. (2015) conducted displacement measurements using various types of sensors, including global positioning systems (GPSs) and wire displacement gauges with a hybrid potentiometer sensor. Huang *et al*. (2018) installed two displacement transducers between the abutment and girder of a cable-stayed bridge. Xia *et al*. (2018) installed four displacement sensors to perform the thermal performance analysis of a suspension bridge. Zhao *et al*. (2019) monitored the longitudinal displacement behavior of an arch bridge using magnetostrictive displacement sensors. Garcia-Sanchez *et al*. (2020) conducted a field experiment using displacement sensors to evaluate their method for assessing longitudinal bridge performance. However, because of the relatively expensive cost of the sensor and difficulties in installation and management, contact-type sensors such as linear variable differential transformers (LVDTs) are primarily used for suspension or cable-stayed bridges, where the number of bridge bearings is limited. However, LVDTs are regarded as inefficient because their measurement accuracy is decreased considerably if a contact object vibrates.

To overcome the disadvantages of contact-type displacement sensors, researchers have attempted to develop a displacement measurement system using new sensors such as the laser Doppler vibrometer (LDV) (Nassif *et al*. 2005, Garg *et al*. 2019, 2020) or GPS (Watson *et al*. 2007, Jo *et al*. 2013, Xu *et al*. 2017, Hussan *et al*. 2018, Kim *et al*. 2018, Casciati and Fuggini 2011, Moschas *et al*. 2013, Yi *et al*. 2013). The LDV is a sensor that measures displacement using the Doppler shift a laser reflected from an object. The GPS determines the location of a local sensor based on the geometric position between a local sensor and satellites. However, neither of these two sensors satisfy the abovementioned four requirements for the displacement measurement of bridge bearings. The high cost of the LDV hinders its installation on multiple piers. In addition, the measurement frequency of the LDV, which is within the high-frequency band from kilohertz to megahertz, allows low-frequency displacements to be measured, such as the displacement of a bridge bearing; however, the measurement is inefficient. Meanwhile, the GPS affords resolution in the centimeter range, which is insufficient for measuring bridge bearing displacement, and communication between a local sensor and satellites may malfunction when the GPS is installed under a bridge girder.

Computer-vision-based approaches can be a viable alternative, whereas contact-type sensors, GPSs, and LDVs are unsuitable for bridge bearing displacement measurement owing to their respective disadvantages. Computer-vision-based displacement measurement allows contactless displacement measurement using relatively inexpensive equipment. Furthermore, in recent years, many computer-vision-based displacement measurement systems for real-world applications have been reported (Lee and Shinozuka 2006, Lee *et al*. 2007, Ye *et al*. 2013, Cho *et al*. 2016, Feng and Feng 2016, Lee *et al*. 2017, Ye *et al*. 2016a). Previous computer-vision-based displacement measurement methods vary in terms of (1) the usage of reference targets, (2) methods for extracting features, and (3) coordinate transformation. Target-based approaches use a reference target with specific patterns, such as circles (Lee and Shinozuka 2006), a checkerboard (Shariati *et al*. 2015), or a random pattern (Ye *et al*. 2016b. By contrast, non-target approaches (Dong *et al*. 2019, Feng *et al*. 2015, Shao *et al*. 2021, Yoon *et al*. 2016) extract trackable features from an image of a structure and trail the moving path of the extracted features. Once trackable features are extracted in an image, coordinate transformation converts the displacement obtained in the image coordinates into real-world coordinates. Several different methods have been employed for coordinate transformation, such as simple scaling (Lee and Shinozuka 2006, Feng *et al*. 2015, Shariati *et al*. 2015), affine transform (Fukuda *et al*. 2010), and homography transform (Sładek *et al*. 2013, Wu *et al*. 2014, Dworakowski *et al*. 2016, Jeong *et al*. 2017, Lee *et al*. 2020). In recent years, a research report enhanced the displacement accuracy by considering camera motion and its thermal effect (Xing *et al*. 2022) and measurement speed (Shrestha *et al*. 2020, Song *et al*. 2022). Other research reports employed drone cameras instead of conventional digital cameras to get closer access to bridge girders or high-rise buildings (Ribeiro *et al*. 2021, Weng *et al*. 2021). Recent advances of machine learning and deep learning models also contributed the advances of computer vision displacement measurement system (Luo *et al*. 2021, Zhu *et al*. 2021). Regardless of the variation, computer vision systems are cost-effective and can facilitate displacement measurement in large-scale civil structural systems.

Herein, a computer-vision-based horizontal displacement measurement system for bridge bearings is proposed. To satisfy the first and second requirements mentioned above, the system was designed with a wireless network topology via a gateway connected to a closed-circuit television (CCTV). The hardware comprises targets, CCTVs, gateways, and a central server. The target is a 50 mm squared target that comprises four large white circles on a black background, and the CCTV was used to capture images of the corresponding target. Compared to the non-target approaches (Dong *et al*. 2019, Feng *et al*. 2015, Shao

et al. 2021, Yoon *et al*. 2016) or the deep learning-based feature extraction method (Zhu *et al*. 2021), the employment of the simple target design aims to stable and robust displacement measurement under the 1-hour measurement interval where the image capturing environment significantly varying from one another. The CCTV model employed in the proposed system is capable of night vision capture, which helps robust 24-hour monitoring compared to the previous works (Feng *et al*. 2015, Xing *et al*. 2022) employing a commercial DSLR cameras. The captured images were sent to the central server via long-term evolution (LTE) networks through a connected gateway, which enables a wide range of monitoring on bridge area.

To satisfy the third requirement, the field of view (FOV) of the CCTV was set wider than the maximum horizontal displacement of the bearing, and the circular Hough transform (CHT) was employed to capture the centers of circles on the target at a submillimeter resolution in the full FOV. It is also required for the proposed system to accurately detect circles in captured images where targets are far apart from each other due to large thermal displacement of bridge bearing. This technical demand is distinct from the ones of the previous works for the real-time measurement (Hoskere *et al*. 2019, Ma *et al*. 2022, Park *et al*. 2010, Ribeiro *et al*. 2021) where targets are close to each other in frames and fast target detection is needed for structural dynamic property observation. The employment of CHT-based target detection algorithm excellently handles this technical demand in the field environment.

To satisfy the fourth requirement, image preprocessing techniques, such as gamma correction and adaptive binarization techniques, were selectively applied to the images from the CCTVs under subpar imaging conditions to enhance the features of the targets. The homography transformation calculated from the four center circles converts the movement of a reference target in an image into a real displacement. The proposed system was implemented on a bridge under operation in Seoul, South Korea. The system comprises 71 CCTVs and targets, 57 temperature sensors, and 40 gateways installed on the bridge, as well as a central server at the authority of the bridge. The stability and accuracy of the system were evaluated using images obtained for 17 days. Error analysis was performed to determine the factors that can deteriorate the accuracy owing to the inevitable field environment.

2. Computer-vision-based displacement measurement system

The proposed system was composed of hardware and algorithms, as illustrated in Fig. 1. It captures the images of the target on the bridge bearings and stores them at a distant central server, and the algorithm analyzes the stored images to obtain the horizontal displacement. In the subsequent section, the hardware and algorithm are explained comprehensively.

2.1 Hardwar

2.1.1 Target

The target is a panel with shapes whose features can be captured accurately by the computer vision algorithm. The targets used in the proposed system were designed as squares with 50-mm-long sides containing four large white circles on a black background, as shown in Fig. 2(a). Each circle has a diameter of 20 mm, which allows the center of the image to be localized using the CHT without any predefined region of interest (RoI). The target was

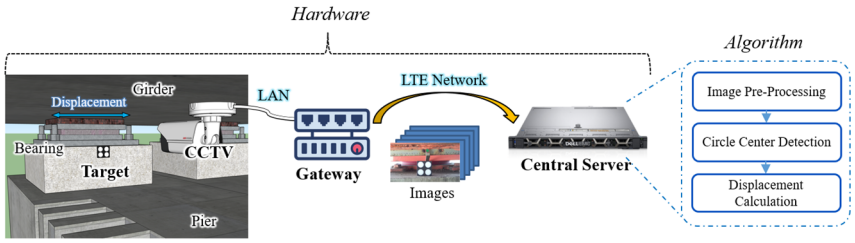

Fig. 1 Hardware and algorithm of proposed system

(a) (b)

Fig. 2 Target of proposed system: (a) design (units: mm); and (b) installation on bridge bearing support

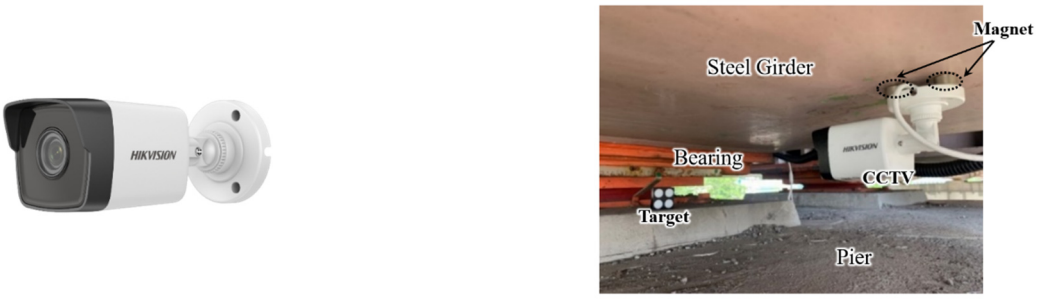

(a) (b)

Fig. 3 CCTV of proposed system: (a) Hikvision DS-2CD1021-I model; and (b) example of installation on bridge

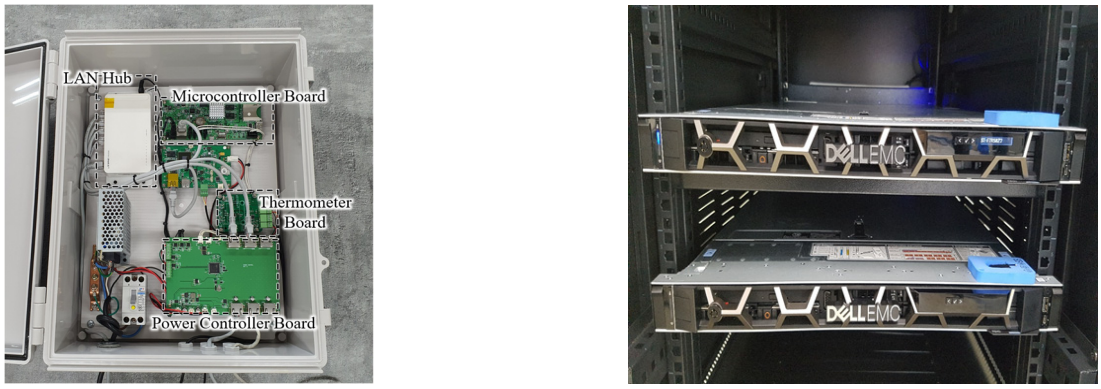

(a) Gateway (b) Central server

Fig. 4 Gateway and central server of proposed system

fabricated using matt acrylic to minimize the effects of rain and light reflection, which will distort the image. During installation on the bridge, all targets were adhered to the bearing support with epoxy, as shown in Fig. 2(b).

2.1.2 CCTV

A CCTV was used as an imaging device to measure displacement using an appropriate image processing algorithm. The CCTV used in the system was Hikvision DS-2CD1021-I, as shown in Fig. 3(a). This model can capture images with full high-definition (HD) resolution (i.e., 1920 × 1080) using a 1/2.7" progressive scan CMOS[1] and has a narrow-angle lens to minimize image distortion. The horizontal field-of-view (FOV) of the CCTV was 90.2° when the focal length was 4 mm. The CCTV model is capable of night vision capture, which enables robust 24-hour monitoring. The CCTV was attached underneath the bridge girder using a magnet to view the target on the bearing support, as shown in Fig. 3(b). Hence, the CCTV traversed horizontally with the girder while the target remained stable; as such, the relative displacement between the girder and bearing support was measured, and it matched exactly the displacement of the bridge bearing. Note that each CCTV was powered by a power cable branched from the main electricity cable for stable and continuous monitoring.

[1] Complementary metal–oxide–semiconductor

2.1.3 Gateway and central server

The gateway communicates with one or more CCTVs to acquire images of targets and transmit the images to the central server via LTE networks. The gateway used in the system comprises a microcontroller board, LAN hub, power controller board, and a thermometer board to measure the ambient temperature in a PVC box enclosure, as shown in Fig. 4(a). The LAN hub is connected to the CCTV as well as a commercial LTE modem outside the gateway to transfer the acquired data to the central server remotely.

The central server of the system (as shown in Fig. 4(b)) is a Dell Power Edge equipped with a 2.1 GHz×1P/16 Core CPU, 32 GB of RAM, 4 TB of storage, and an NVIDIA Quadro K420. It was installed at the authority of the bridge and stored images transferred via the Internet. The server was equipped with software to process the stored images based on the algorithm, which will be described next, to obtain the horizontal displacement of the bridge bearings.

2.2 Algorithm

Fig. 5 shows the overall procedure of the proposed displacement measurement algorithm. The proposed algorithm primarily involves configuration setup, image preprocessing, circle center detection, and displacement calculation. The configuration setup includes a gamma correction factor, the application of adaptive binarization, the target circle radius range, and the target circle size in the world coordinate system (WCS). Each configuration setup

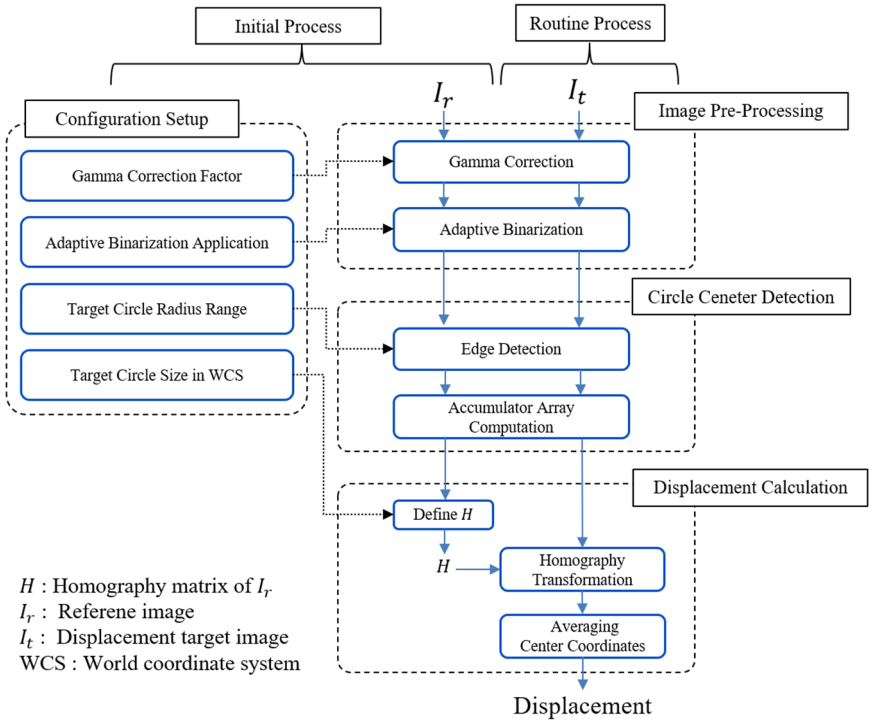

Fig. 5 Overall procedure of displacement measurement algorithm

(a) (b) (c)

Fig. 6 Image preprocessing examples: (a) Original image; (b) gamma correction on (a); (c) adaptive image binarization on (b)

was used for the related processes in image preprocessing, circle center detection, and displacement calculation. In Fig. 5, the related processes are shown as connected to each configuration setup via dotted lines. To enhance the circular features on a target, gamma correction and adaptive image binarization are applied to an image based on the configuration during image preprocessing. Circle center detection localizes four circles on a target. First, the circle center detection identifies the edges of an object in an image and selects the center coordinates via accumulator array computation (AAC). In the displacement calculation, the homography matrix H between the image coordinate system (ICS) and WCS is defined using a reference image, I_r. Subsequently, homography transformation using H is performed to convert the ICS circle coordinates to the WCS in the other target images, I_t, to measure the displacement in real-world units (e.g., mm). The configuration setup, where H and its proceeding steps are defined, is known as the initial process as it is performed only once in the proposed algorithm. The abovementioned process is repeated for every target image in a dataset to measure the displacement for a specific duration.

2.2.1 Image preprocessing

The real-world environment may include many unexpected factors or obstacles that deteriorate the circle detection accuracy. To minimize the possibility of accuracy deterioration, image preprocessing steps were incorporated prior to the CHT. The image preprocessing options used in this study were 1) gamma correction and 2) adaptive image binarization. Gamma correction was performed to darken the unnecessary areas for circle detection. As shown in Fig. 6(b), the white area of the circles remained after gamma correction and the original image darkened. In addition, most of the objects around the bridge bearings became invisible after gamma correction was performed. Adaptive image binarization following gamma correction was performed to enhance the border of the circles in the image. As shown in Fig. 6(c), the adaptive image binarization emphasized the border of the circle.

2.2.2 Circle detection algorithm for reference target detection

The circle detection used in this study was a re-implementation of the "imfindcircles" (MATLAB, 2021) function in MATLAB and is based on work of Atherton and

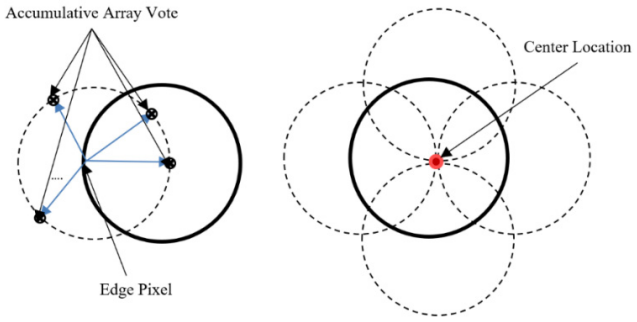

Fig. 7 Accumulator array computation of circular Hough transformation

Kerbyson (1999). This section presents the core aspects of the circle-detection algorithm. The circle detection algorithm is composed of two main steps: edge detection and accumulator array computation. The final step radius estimation is performed only when visualization is required.

In the first step, i.e., edge detection, edges in an image are identified using Sobel edge detection (Kanopoulos *et al.* 1988). In the second step, AAC is performed on the pixels of the detected edge. As shown in Fig. 7, the ACC draws circles with a radius within a predetermined range on the edges, and then accumulates votes on the pixels at the end of the radius. If the detected edges form a circle, as depicted in Fig. 7, then many votes will be cast to the center point, as highlighted by a red dot in Fig. 7. The center point of the circle is obtained by selecting pixels whose votes exceed a certain threshold or the local maximum of a selected algorithm. To explain the final step, radius estimation is not included because the subsequent homography transformation requires only the centers of the circles. Radius estimation is only necessitated when visualizing the detected circles in an image.

Fig. 8 shows a reference target detection process using the CHT in four steps. Fig. 8(a) shows the original image of a reference target captured by a CCTV. Before the CHT is applied, image preprocessing is performed using the parameters assigned to each CCTV (refer to Section 2.2.1). After image preprocessing is performed, edge detection identifies pixels with a strong intensity change, as shown in Fig. 8(b). Along the pixels determined as edges, ACC is performed to vote for the location of the center points of the circles. Fig. 8(c) shows the accumulation results of ACC in Fig. 8(b). Fig. 8(c) shows four areas whose values are higher compared with the other pixels. The center points of the four areas were selected as the centers of the four circles in the image. Fig. 8(d) shows the circle detection result, where the centers and edges of the circles are highlighted as blue dots and green lines, respectively.

2.2.3 Displacement measurement using homography transformation

Homography transformation is performed to define the relationship between two different planes. Fig. 9 conceptually illustrates the displacement measurement process using homography transformation. The left target in Fig. 9 is a zero-point displacement measurement, and the right target is the location to measure the displacement. It is assumed that the target moves on a two-dimensional plane that is based on the ICS. A homography matrix is obtained by defining the transformation relationship between the image coordinate system and the WCS. Because the WCS is another two-dimensional plane, the relationship between the two planes is defined as a projection. Therefore, the homography matrix between the two planes is defined as the projection relationship among the four blue marks on the ICS and the other four blue marks on the WCS. The projection relationship defined between ICS and WCS is used to transform the coordinates of the ICS into a WCS. The equation of homographic relationship between ICS and WCS is defined as

$$sI_{3\times1} = H_{3\times3}W_{3\times1} \tag{1}$$

where s denotes scaling factor, $I_{3\times1} = [u\ v\ 1]^{\mathrm{T}}$ denotes

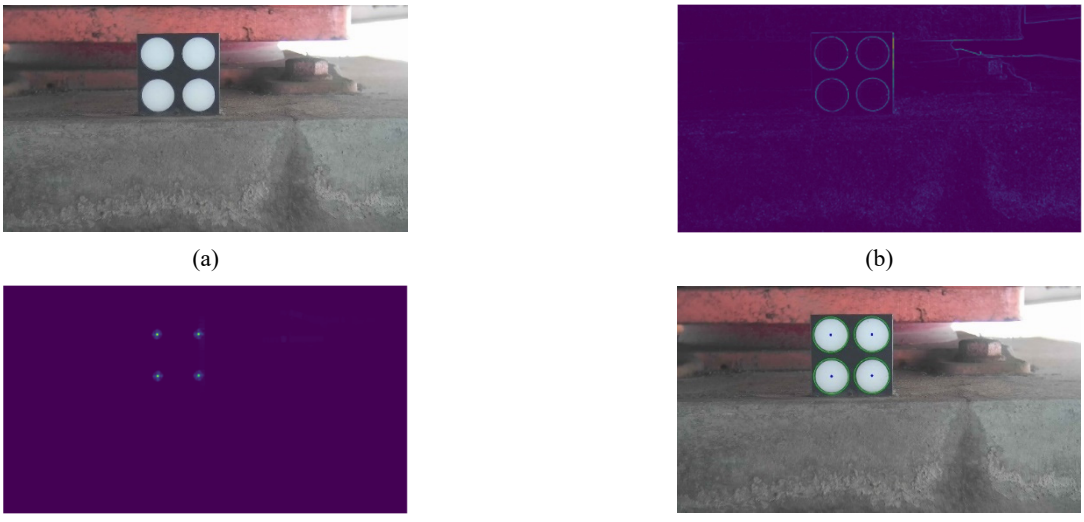

(a) (b) (c) (d)

Fig. 8 Circular Hough transformation examples: (a) Original image; (b) Sobel edge detection; (c) accumulator array computation; (d) center and radius estimation

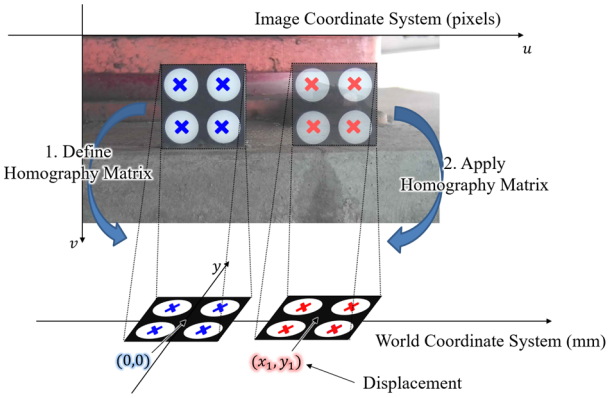

Fig. 9 Displacement measurement using homography transformation

ICS, $H_{3\times3}$ denotes the homography matrix, and $W_{3\times1} = [x\ y\ 1]^{\mathrm{T}}$ denotes WCS. The scaling factor is set to 1 to use the exact projective relationship between ICS and WCS. In ICS, u, and v are respectively denotes horizontal and vertical coordinates, while x, and y denotes horizontal and vertical coordinates in WCS. The four red marks in the ICS are converted to the WCS system. After conversion, the average of the coordinates of the four points in the world coordinate system is determined as the displacement of the target. This is because the target at the initial zero-point position is projected to the (0, 0) on the WCS; therefore, the coordinates of the other points are displacements in the x- and y-axis directions, separately. The ICS uses pixels as the coordinate system unit because it represents an image, whereas the WCS uses the millimeter system to indicate the actual moving distance of the target.

3. Field Experiment

3.1 Test bridges and system installation

The developed system was installed on the Tancheon overpass located in Seoul, South Korea, an overview of which is shown in Fig. 10. Fig. 11 shows the layout of the sensor setup of the Tancheon overpass for a field experiment. 1. CCTVs were installed at both ends of the inspection target girders, P1, P9, P24, P27, P34, P41, P55, P59, where bridge bearings are concerned for poor condition. In Fig. 11, bridge bearings, CCTVs, bridge

Fig. 10 Overview of Tancheon overpass

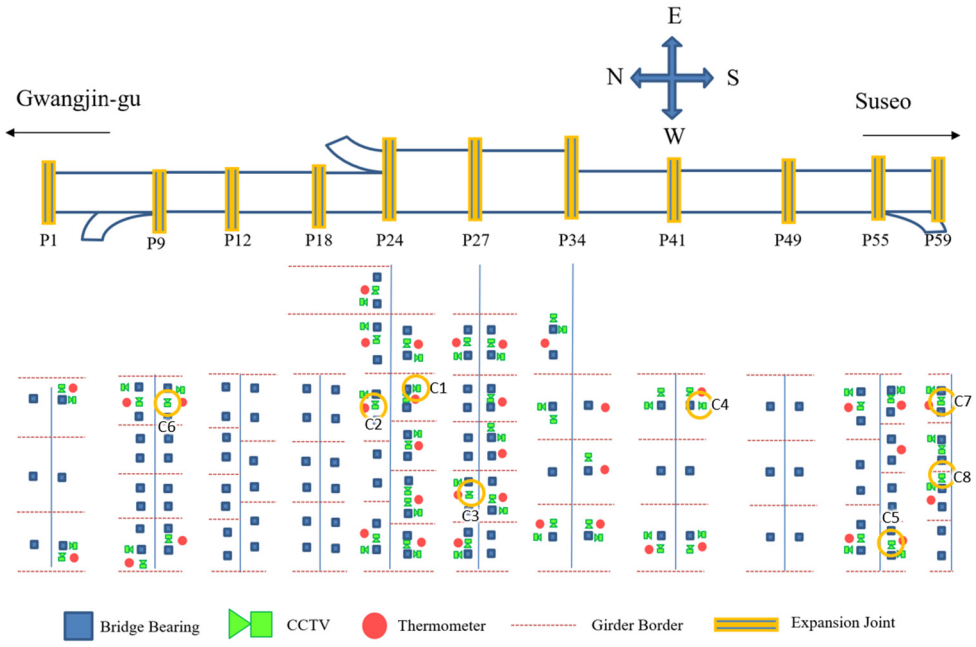

Fig. 11 Overview of sensor setups on test bed

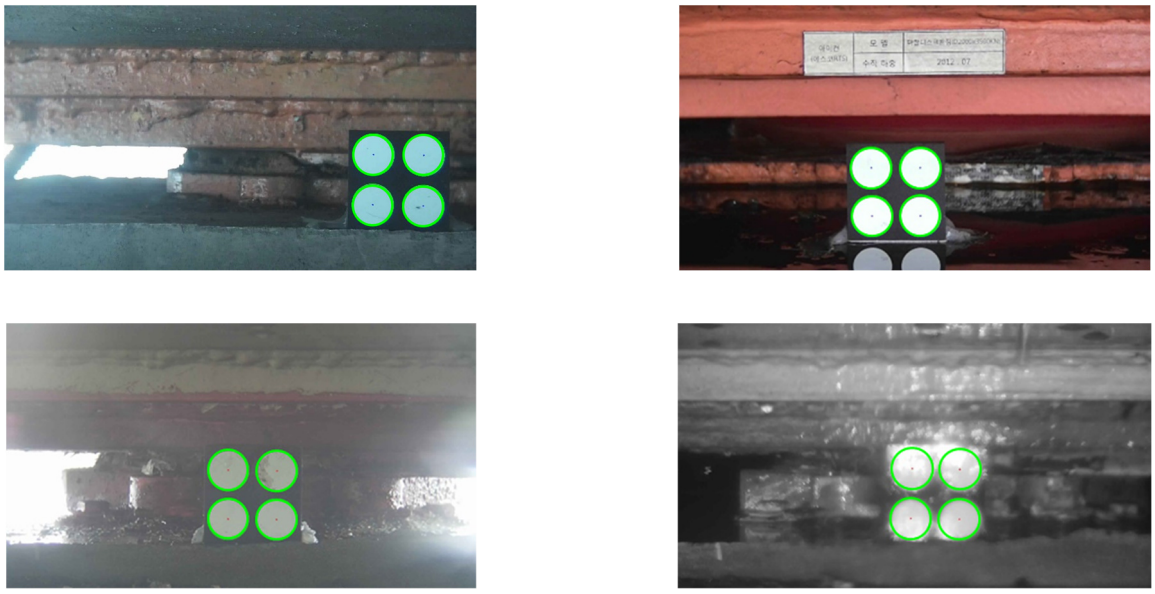

(c) (d)

Fig. 12 Example of successful circle detection: (a) C3, 08:00 on November 24th; (b) C4, 09:00 on November 19th; (c) C5, 13:00 on September 7th; (d) C5, 06:00 on November 19th

expansions and thermometers are marked as blue squares, green camera icons, yellow rectangles, and red circles, respectively. The thermometers were installed to facilitate further studies involving temperature–displacement analysis, which is outside the scope of this study. Eight CCTVs were selected and denoted as C1–C8. C1–C5 were selected as examples of circle detection *success* and *failure*, and C6–C8 were used to evaluate the accuracy of displacement measurement.

3.2 Robustness of circle center detection in field environment

Circular detection was performed using the proposed method based on the parameters selected for each CCTV (see Table A3 in the Appendix). The detection was performed using 71 CCTVs installed on the Tancheon overpass. The test images were captured once every hour for 17 days from 1:00 on November 15, 2020, to 17:00 on December 1, 2020, and 28,542 images were used for the test. After performing circle detection on all images, their numbers and locations were analyzed. If the number of detected circles is four and their locations yield a parallelogram, then the detection of the image is evaluated as "*success*." If neither condition is satisfied, then the detection of the image is evaluated as "*failure*." Among all the images, the number of failed images was 48 (0.168%). For details regarding the experimental results, please refer to Tables A1 and A2 in the Appendix.

Fig. 12 shows an image in which a circle is successfully detected. Fig. 12(a) shows the results of circle detection under relatively favorable capturing conditions. As shown in Fig. 12(b), the proposed algorithm successfully detected the four circles in the target despite the reflection on the water puddle due to heavy rain. Fig. 12(c) shows that the proposed algorithm successfully detected a circle despite the intense backlit. Fig. 12(d) shows that the circles were detected even though the image was blurred by water on the camera lens and the target.

The failures were investigated based on the fault images presented in Fig. 13. As shown in Fig. 13(a), C1 was installed on the Tancheon overpass. A bird appeared in the FOV of the CCTV and screened out one of the circles on the target. Meanwhile, the image shown in Fig. 13(b) was assumed to be completely due to the intense backlight, which often occurs when the sun appears in the FOV. However, in most cases, the image quality was sufficient for circle detection. Fig. 13(c) shows a significant contrast difference, which resulted in a failed circle detection in the bottom row. The sunlight was illuminated directly on the bottom row, which resulted in the subpar performance of the Sobel edge detector. As shown in Fig. 13(d), the circular shape of the target could not be preserved owing to the reflection on the wet surface due to rain. Because the failure occurred in C5 on November 19th and November 22nd, which were rainy days, the target is required to be shifted to a dry location. As shown in Fig. 13, the failures were recorded primarily from subpar abnormal images affected by heavy rain or intense backlight. The algorithm proved to be effective in most of the imaging conditions, as indicated by the failure rate of 0.168%.

3.3 Accuracy of measured displacement

To evaluate the accuracy of the displacements measured using the proposed system, the ground-truth displacement was measured by human inspectors using analog displacement meters (ADMs) (Fig. 14(a)). The images near the target were captured by the CCTVs, and the markings on a ruler pointed by the pointer were read manually. The ADM comprised a steel ruler and a small pointer, which indicate the displacement, as shown in Fig. 14(b). The

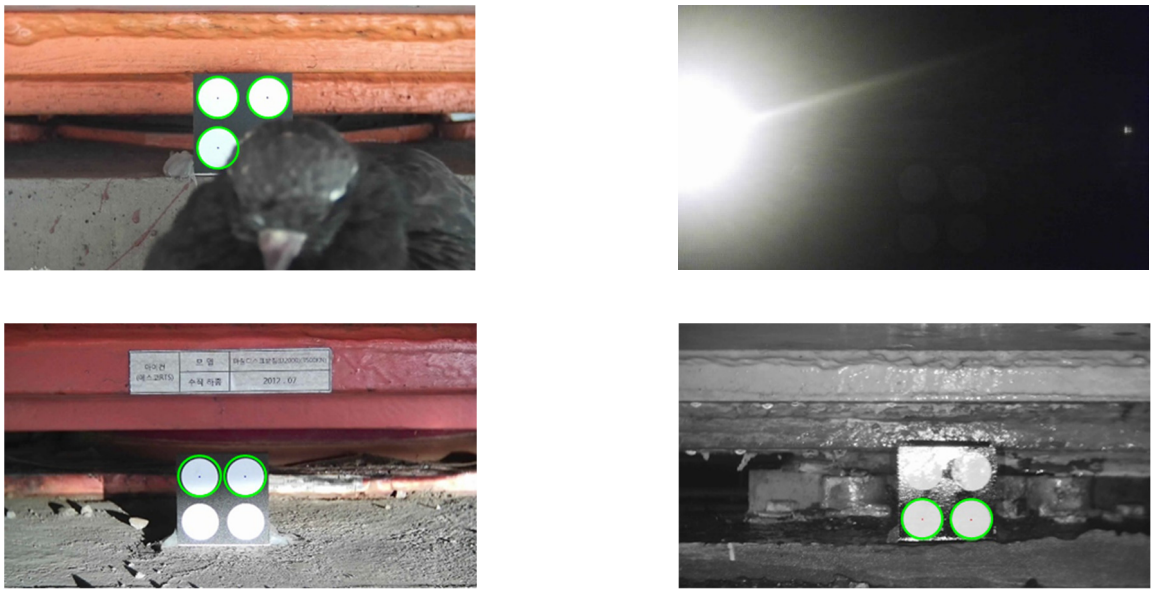

(c) (d)

Fig. 13 Examples of faults in circle detection: (a) Bird appeared in FOV (C1, 15:00 on November 29th); (b) target image affected by backlight (C2, 07:00 on November 20th); (c) significant contrast difference between upper and lower sections of target (C4, 08:00 on December 1st); (d) circle shapes lost due to reflection of wet surface (C5, 7:00 on November 22)

(a) (b)

Fig. 14 Installation of analogue displacement meter setup: (a) wide view; and (b) close view

ADMs were installed at three locations next to the CCTVs, i.e., C6–C8.

Fig. 15 shows the displacement measured by the ADMs and proposed system. All displacement data were corrected by calibrating the displacements at 1:00 on November 15 to zero. As shown in Figs. 15(a)-(c), the displacements measured by the proposed system for 17 days were similar to those measured by the ADMs. The measured displacements during the 17 days have a large range of about 35 mm. Figs. 15(d)-(f) show the errors between the displacements measured by the proposed system and the ADMs. The errors in the three graphs were distributed near 0 mm, and the maximum errors were 0.3636, 0.3610, and 0.2716 mm, respectively. C6, C7, and C8 indicated root-mean-square errors of 0.1120, 0.1444, and 0.1353 mm, respectively. The error of the total data was 0.10 mm on average. The experimental results show that the proposed displacement measurement algorithm measured the displacement of the bridge bearing with an accuracy within 0.1 mm of the average error.

On the comparison with one of the RoI-based displacement measurement method (Feng and Feng 2016), the error is calculated as normalized root mean squared error (NRMSE) of which equation is defined as follow

$$\text{NRMSE} = \frac{\sqrt{\frac{1}{n}\sum_i^n (x_i - y_i)^2}}{y_{\max} - y_{\min}} \tag{2}$$

where n is number of measurement data, x_i is the ith displacement data measured by the proposed system, $y_i$is the ith ground truth data. The proposed system showed NRMSE 0.411%, 0.466%, and 0.508% on C6, C7, and C8 respectively, while the previous work (D. Feng *et al.* 2016) reported NRMSE 0.72% overall in the laboratory-scale test. The experimental case convinces the robustness of the proposed algorithm since the proposed system achieved lower NRMSE while operating under field environment without predefined RoI.

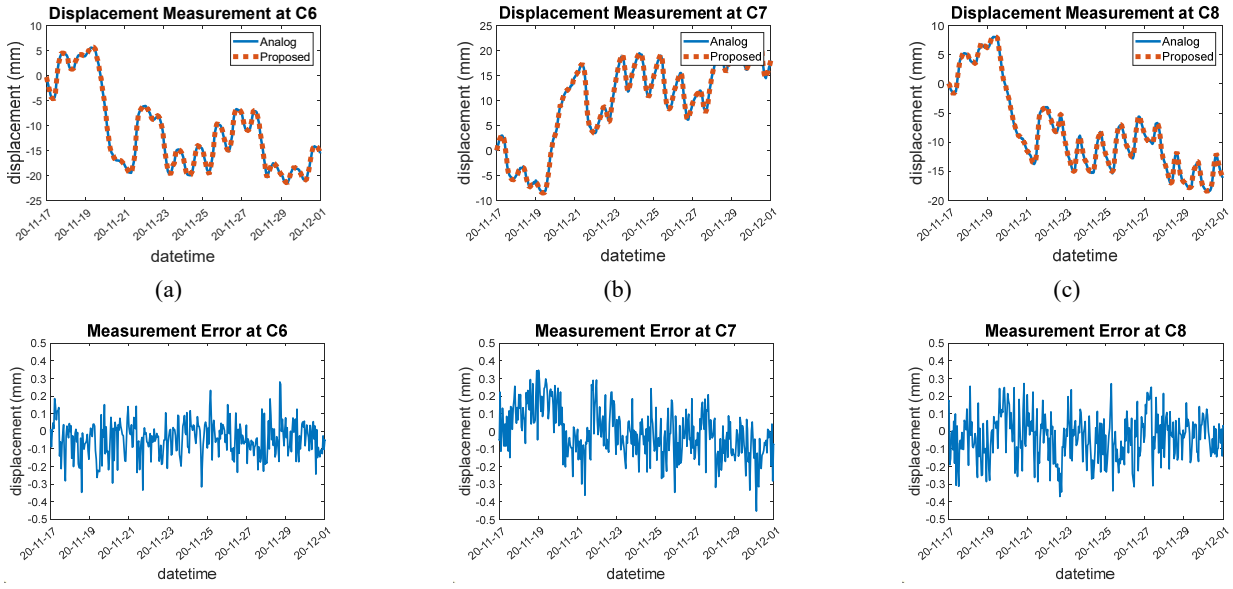

Fig. 15 Comparison of displacement data measured using analog displacement meter and algorithm: (a)–(c) displacement measurement result; and (d)–(f) measurement error

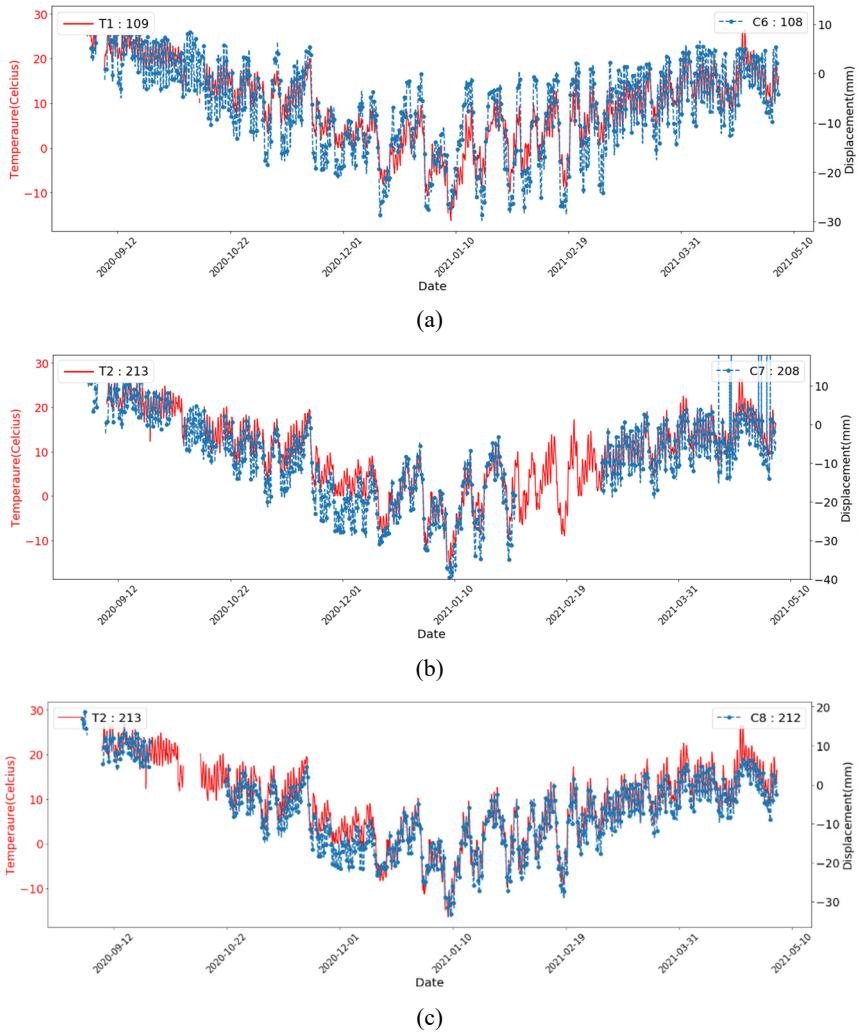

Fig. 16 Long-term horizontal bridge bearing displacement (blue dotted line) and temperature (red solid line) measured by proposed system at (a) C6; (b) C7; and (c) C8

3.4 Long-term displacement and temperature monitoring

Fig. 16 shows the long-term horizontal bridge bearing displacement measured using the proposed system at C6–C8. The results of the long-term measurement experiment show that the proposed system accurately measured large displacements caused by the seasonal change, ranging about 50 mm, in the order of submillimeter. During the measurement period, the temperature data ranged from approximately 30°C to -10°C, which encompassed the temperature range experienced by the bridge during its operation. The experimental results obtained from 8-month-long measurements show that the proposed system can be used for long-term monitoring for more than one year, including the maximum displacement range.

In addition, the proposed system can perform displacement measurement while maintaining continuity with previous data when the measurement halts for various reasons. The displacement data at C6 shown in Fig. 16(a) were measured without discontinuity. However, for the displacement data of C7 and C8 shown in Figs. 16(b) and 16(c), displacement measurement was halted at certain periods. The measurement interruption shown in both Figs. 16(b) and 16(c) in September 2020 was due to the verification of the system stability. The cause of the measurement interruption shown in Fig. 16(b) on February 2021 was assumed to be an LTE communication error; the interruption was restored in March 2021 during a regular inspection. However, after the interruption, the proposed system continued to measure the displacement along with the previous data based on the initially set reference point. The computer-vision-based displacement measurement of the proposed system can operate stably in an environment comprising civil structures, although measurement may be interrupted because of uncertain reasons.

4. Conclusions

A computer-vision-based bridge expansion displacement measurement system was proposed herein. The proposed system comprised hardware and an algorithm. The hardware included a reference target, CCTV, and central server. The reference target was a square measuring 50 mm × 50 mm that was fabricated using matt acrylic to prevent water and damage. The displacement measurement algorithm comprised three steps: image preprocessing, circle center detection, and displacement calculation. During image preprocessing, gamma correction and adaptive image binarization were selectively applied to enhance the features of the circles on the target. The circle center detection involved a CHT-based algorithm that localized the circle centers on a four-point target. The location of the target identified via the circle center detection was converted to real-world displacement via homography transformation in the displacement calculation step. The proposed displacement measurement algorithm successfully handles the technical demand of robust target detection under large displacement change in the field environment.

Field experiments were conducted on the Tancheon Overpass to evaluate the accuracy of the proposed algorithm. First, 28,542 images acquired from 71 CCTVs from November 15 to December 1, 2020 were used to evaluate the circle detection accuracy. Among all the test images, 48 images indicated errors, with an error rate of approximately 0.168%. Additionally, another experiment was conducted to evaluate the displacement measurement performance of the proposed algorithm. Ground-truth data were obtained from November 15 to December 1, 2020 using analog displacement meters installed on three CCTVs. The displacement changes during experimental period reach up to 35 mm including 25 mm displacement change within two days. For the three CCTVs used in the experiment, the displacement of the algorithm and the ground-truth displacement showed similar values during the experimental period. An average error of 0.10 mm demonstrated the excellency of the large displacement measurement capability of the proposed system. The long-term measurement capability of the proposed system was evaluated via an 8-month-long measurement experiment. The proposed system consistently measured the bridge bearing displacement without any further modification of the algorithm. The maximum displacement change during 8-month-long measurement is about 40mm, which reconfirms the large displacement capability of the proposed system. The long-term experiment demonstrated the stability and repairability of the proposed system under harsh civil structure environments.

The proposed system is cost-effective due to low-cost sensors, wireless communication, and facilitated installation. The CCTV model employed in the proposed system costs less than $100, while the comparable LVDT models cost about $500. With the help of the wireless communication, the proposed system can save labor and cost for the cable installation to connect each sensor to the server on the long multi-span bridges. Furthermore, the computer vision sensor with a marker does not require labor and cost for the sensor alignment, which is very critical for the contact-type displacement sensors. Thus, the proposed system would help to build the cost-effective and accurate bridge bearing monitoring system on various bridges.

Acknowledgments

This study was supported by the Korea Agency for Infrastructure Technology Advancement (KAIA), grant funded by the Ministry of Land, Infrastructure, and Transport (Grant 21CTAP-C163726-01).

References

Atherton, T.J. and Kerbyson, D.J. (1999), "Size invariant circle detection", *Image Vision Comput.*, **17**(11), 795-803. https://doi.org/10.1016/s0262-8856(98)00160-7

Casciati, F. and Fuggini, C. (2011), "Monitoring a steel building using GPS sensors", *Smart Struct. Syst., Int. J.*, **7**(5), 349-363. https://doi.org/10.12989/SSS.2011.7.5.349

Cho, S., Park, J.W., Palanisamy, R.P. and Sim, S.H. (2016), "Reference-free displacement estimation of bridges using

Kalman filter-based multimetric data fusion", *J. Sensors*, 2016. https://doi.org/10.1155/2016/3791856

Dong, C.Z., Celik, O. and Catbas, F.N. (2019), "Marker-free monitoring of the grandstand structures and modal identification using computer vision methods", *Struct. Health Monitor.*, **18**(5-6), 1491-1509. https://doi.org/10.1177/1475921718806895/ASSET/IMAGES/LARGE/10.1177_1475921718806895-FIG2.JPEG

Dworakowski, Z., Kohut, P., Gallina, A., Holak, K. and Uhl, T. (2016), "Vision-based algorithms for damage detection and localization in structural health monitoring", *Struct. Control Health Monitor.*, **23**(1), 35-50. https://doi.org/10.1002/stc.1755

Federal Highway Administration (2007), Load and Resistance Factor Design (LRFD) for Highway Bridge Superstructures REFERENCE MANUAL.

Feng, D. and Feng, M.Q. (2016), "Vision-based multipoint displacement measurement for structural health monitoring", *Struct. Control Health Monitor.*, **23**(5), 876-890. https://doi.org/10.1002/stc.1819

Feng, M.Q., Fukuda, Y., Feng, D. and Mizuta, M. (2015), "Nontarget Vision Sensor for Remote Measurement of Bridge Dynamic Response", *J. Bridge Eng.*, **20**(12), 04015023. https://doi.org/10.1061/(asce)be.1943-5592.0000747

Find circles using circular Hough transform - MATLAB imfindcircles (n.d.), Retrieved May 31, 2021, from https://www.mathworks.com/help/images/ref/imfindcircles.html

Fukuda, Y., Feng, M.Q. and Shinozuka, M. (2010), "Cost-effective vision-based system for monitoring dynamic response of civil engineering structures", *Struct. Control Health Monitor.*, **17**(8), 918-936. https://doi.org/10.1002/stc.360

Garcia-Sanchez, D., Fernandez-Navamuel, A., Sánchez, D.Z., Alvear, D. and Pardo, D. (2020), "Bearing assessment tool for longitudinal bridge performance", *J. Civil Struct. Health Monitor.*, **10**, 1023-1036. https://doi.org/10.1007/s13349-020-00432-1

Garg, P., Moreu, F., Ozdagli, A., Taha, M.R. and Mascareñas, D. (2019), "Noncontact dynamic displacement measurement of structures using a moving laser Doppler vibrometer", *J. Bridge Eng.*, **24**(9), 04019089. https://doi.org/10.1061/(asce)be.1943-5592.0001472

Garg, P., Nasimi, R., Ozdagli, A., Zhang, S., Mascarenas, D.D.L., Reda Taha, M. and Moreu, F. (2020), "Measuring transverse displacements using unmanned aerial systems laser doppler vibrometer (UAS-LDV): Development and field validation", *Sensors*, **20**(21), 1-16. https://doi.org/10.3390/s20216051

Guo, T., Liu, J., Zhang, Y. and Pan, S. (2015), "Displacement Monitoring and Analysis of Expansion Joints of Long-Span Steel Bridges with Viscous Dampers", *J. Bridge Eng.*, **20**(9), 04014099. https://doi.org/10.1061/(ASCE)BE.1943

Hoskere, V., Asce, S.M., Park, J.-W., Yoon, H., Asce, A.M., Spencer, B.F. and Asce, F. (2019), "Vision-Based Modal Survey of Civil Infrastructure Using Unmanned Aerial Vehicles", *J. Struct. Eng.*, **145**(7), 04019062. https://doi.org/10.1061/(ASCE)ST.1943-541X.0002321

Huang, H.-B., Yi, T.-H., Li, H.-N. and Liu, H. (2018), "New Representative Temperature for Performance Alarming of Bridge Expansion Joints through Temperature-Displacement Relationship", *J. Bridge Eng.*, **23**(7), 04018043. https://doi.org/10.1061/(asce)be.1943-5592.0001258

Hussan, M., Kaloop, M.R., Sharmin, F. and Kim, D. (2018), "GPS Performance Assessment of Cable-Stayed Bridge using Wavelet Transform and Monte-Carlo Techniques", *KSCE J. Civil Eng.*, **22**(11), 4385-4398. https://doi.org/10.1007/s12205-018-0438-3

Jeong, Y., Park, D. and Park, K.H. (2017), "PTZ camera-based displacement sensor system with perspective distortion correction unit for early detection of building destruction", *Sensors*, **17**(3), 430. https://doi.org/10.3390/s17030430

Jo, H., Sim, S.H., Tatkowski, A., Spencer, B.F. and Nelson, M.E. (2013), "Feasibility of displacement monitoring using low-cost GPS receivers", *Struct. Control Health Monitor.*, **20**(9), 1240-1254. https://doi.org/10.1002/stc.1532

Kanopoulos, N., Vasanthavada, N. and Baker, R.L. (1988), "Design of an Image Edge Detection Filter Using the Sobel Operator", *IEEE J. Solid-State Circuits*, **23**(2), 358-367. https://doi.org/10.1109/4.996

Kim, K., Choi, J., Chung, J., Koo, G., Bae, I.H. and Sohn, H. (2018), "Structural displacement estimation through multi-rate fusion of accelerometer and RTK-GPS displacement and velocity measurements", *Measurement: J. Int. Measure. Confed.*, **130**, 223-235. https://doi.org/10.1016/j.measurement.2018.07.090

Korean Authority of Land and Infrastructure Safety (2019), Detailed guidelines for safety and maintenance of infrastructures (Bridges).

Lee, J.J. and Shinozuka, M. (2006), "A vision-based system for remote sensing of bridge displacement", *NDT and E Int.*, **39**(5), 425-431. https://doi.org/10.1016/j.ndteint.2005.12.003

Lee, J.J., Fukuda, Y., Shinozuka, M., Cho, S. and Yun, C.-B. (2007), "Development and application of a vision-based displacement measurement system for structural health monitoring of civil structures", *Smart Struct. Syst., Int. J.*, **3**(3), 373-384. https://doi.org/10.12989/sss.2007.3.3.373

Lee, J., Lee, K.C., Cho, S. and Sim, S.H. (2017), "Computer vision-based structural displacement measurement robust to light-induced image degradation for in-service bridges", *Sensors*, **17**(10), 2317. https://doi.org/10.3390/s17102317

Lee, J., Lee, K.C., Jeong, S., Lee, Y.J. and Sim, S.H. (2020), "Long-term displacement measurement of full-scale bridges using camera ego-motion compensation", *Mech. Syst. Signal Process.*, **140**, 106651. https://doi.org/10.1016/J.YMSSP.2020.106651

Luo, L., Feng, M.Q., Wu, J. and Bi, L. (2021), "Modeling and detection of heat haze in computer vision based displacement measurement", *Measurement*, **182**, 109772. https://doi.org/10.1016/J.MEASUREMENT.2021.109772

Ma, Z., Choi, J. and Sohn, H. (2022), "Real-time structural displacement estimation by fusing asynchronous acceleration and computer vision measurements", *Comput.-Aided Civil Infrastr. Eng.*, **37**(6), 688-703. https://doi.org/10.1111/MICE.12767

Moschas, F., Psimoulis, P.A. and Stiros, S.C. (2013), "GPS/RTS data fusion to overcome signal deficiencies in certain bridge dynamic monitoring projects", *Smart Struct. Syst., Int. J.*, **12**(4), 1738-1991. https://doi.org/10.12989/sss.2013.12.3_4.251

Nassif, H.H., Gindy, M. and Davis, J. (2005), "Comparison of laser Doppler vibrometer with contact sensors for monitoring bridge deflection and vibration", *NDT and E Int.*, **38**(3), 213-218. https://doi.org/10.1016/j.ndteint.2004.06.012

Park, C. and Lee, H. (2016), "Prediction on domestic transportation infrastructure maintenance investment", Construction Economy Research Institute of Korea. http://www.cerik.re.kr/report/issue/detail/1964

Park, J.W., Lee, J.J., Jung, H.J. and Myung, H. (2010), "Vision-based displacement measurement method for high-rise building structures using partitioning approach", *NDT & E Int.*, **43**(7), 642-647. https://doi.org/10.1016/J.NDTEINT.2010.06.009

Ribeiro, D., Santos, R., Cabral, R., Saramago, G., Montenegro, P., Carvalho, H., Correia, J. and Calçada, R. (2021), "Non-contact structural displacement measurement using Unmanned Aerial Vehicles and video-based systems", *Mech. Syst. Signal Process.*, **160**, 107869. https://doi.org/10.1016/J.YMSSP.2021.107869

Shao, Y., Li, L., Li, J., An, S. and Hao, H. (2021), "Computer vision based target-free 3D vibration displacement measurement of structures", *Eng. Struct.*, **246**, 113040.

https://doi.org/10.1016/J.ENGSTRUCT.2021.113040
Shariati, A., Schumacher, T. and Ramanna, N. (2015), "Eulerian-based virtual visual sensors to detect natural frequencies of structures", *J. Civil Struct. Health Monitor.*, **5**(4), 457-468. https://doi.org/10.1007/s13349-015-0128-5
Shrestha, A., Dang, J., Nakajima, K. and Wang, X. (2020), "Image processing–based real-time displacement monitoring methods using smart devices", *Struct. Control Health Monitor.*, **27**(2), e2473. https://doi.org/10.1002/STC.2473
Sładek, J., Ostrowska, K., Kohut, P., Holak, K., Gąska, A. and Uhl, T. (2013), "Development of a vision based deflection measurement system and its accuracy assessment", *Measurement*: *J. Int. Measure. Confed.*, **46**(3), 1237-1249. https://doi.org/10.1016/j.measurement.2012.10.021
Song, Q., Wu, J., Wang, H., An, Y. and Tang, G. (2022), "Computer vision-based illumination-robust and multi-point simultaneous structural displacement measuring method", *Mech. Syst. Signal Process.*, **170**, 108822. https://doi.org/10.1016/J.YMSSP.2022.108822
Watson, C., Watson, T. and Coleman, R. (2007), "Structural Monitoring of Cable-Stayed Bridge: Analysis of GPS versus Modeled Deflections", *J. Survey. Eng.*, **133**(1), 23-28. https://doi.org/10.1061/(asce)0733-9453(2007)133:1(23)
Weng, Y., Shan, J., Lu, Z., Lu, X. and Spencer, B.F. (2021), "Homography-based structural displacement measurement for large structures using unmanned aerial vehicles", *Comput.-Aided Civil Infrastr. Eng.*, **36**(9), 1114-1128. https://doi.org/10.1111/MICE.12645
Wu, L.J., Casciati, F. and Casciati, S. (2014), "Dynamic testing of a laboratory model via vision-based sensing", *Eng. Struct.*, **60**, 113-125. https://doi.org/10.1016/j.engstruct.2013.12.002
Xia, Q., Zhou, L. and Zhang, J. (2018), "Thermal performance analysis of a long-span suspension bridge with long-term monitoring data", *J. Civil Struct. Health Monitor.*, **8**(4), 543-553. https://doi.org/10.1007/s13349-018-0299-y
Xing, L., Dai, W. and Zhang, Y. (2022), "Improving displacement measurement accuracy by compensating for camera motion and thermal effect on camera sensor", *Mech. Syst. Signal Process.*, **167**, 108525. https://doi.org/10.1016/J.YMSSP.2021.108525
Xu, Y., Brownjohn, J.M.W., Hester, D. and Koo, K.Y. (2017), "Long-span bridges: Enhanced data fusion of GPS displacement and deck accelerations", *Eng. Struct.*, **147**, 639-651. https://doi.org/10.1016/j.engstruct.2017.06.018
Ye, X.W., Ni, Y.Q., Wai, T.T., Wong, K.Y., Zhang, X.M. and Xu, F. (2013), "A vision-based system for dynamic displacement measurement of long-span bridges: algorithm and verification", *Smart Struct. Syst., Int. J.*, **12**(3_4), 363-379. https://doi.org/10.12989/SSS.2013.12.3_4.363
Ye, X.W., Dong, C.Z. and Liu, T. (2016a), "Image-based structural dynamic displacement measurement using different multi-object tracking algorithms", *Smart Struct. Syst., Int. J.*, **17**(6), 935-956. https://doi.org/10.12989/sss.2016.17.6.935
Ye, X.W., Yi, T.H., Dong, C.Z. and Liu, T. (2016b), "Vision-based structural displacement measurement: System performance evaluation and influence factor analysis", *Measurement*: *J. Int. Measure. Confed.*, **88**, 372-384. https://doi.org/10.1016/j.measurement.2016.01.024
Yi, T.H., Li, H.N. and Gu, M. (2013), "Wavelet based multi-step filtering method for bridge health monitoring using GPS and accelerometer", *Smart Struct. Syst., Int. J.*, **11**(4), 331-348. https://doi.org/10.12989/SSS.2013.11.4.331
Yoon, H., Elanwar, H., Choi, H., Golparvar-Fard, M. and Spencer, B.F. (2016), "Target-free approach for vision-based structural system identification using consumer-grade cameras", *Struct. Control Health Monitor.*, **23**(12), 1405-1416. https://doi.org/10.1002/STC.1850
Zhao, H., Ding, Y., Nagarajaiah, S. and Li, A. (2019), "Longitudinal displacement behavior and girder end reliability of a jointless steel-truss arch railway bridge during operation", *Appl. Sci.*, **9**(11), 2222. https://doi.org/10.3390/app9112222
Zhu, J., Zhang, C., Lu, Z. and Li, X. (2021), "A multi-resolution deep feature framework for dynamic displacement measurement of bridges using vision-based tracking system", *Measurement*, **183**, 109847. https://doi.org/10.1016/J.MEASUREMENT.2021.109847

HJ

Appendix

A-1. Supportive materials for experimental results

Table 1A Number of errors by CCTVs

CCTV No.	No. of errors	CCTV No.	No. of errors	CCTV No.	No. of errors
035	0	119	0	168	1
038	0	120	0	171	0
041	0	123	0	172	0
044	0	124	0	175	0
047	1	128	0	176	0
050	0	131	1	179	0
062	4	132	0	180	0
065	0	135	0	183	1
068	0	136	2	184	0
071	25	139	0	187	0
074	0	140	0	188	0
077	1	143	0	191	0
093	0	144	0	192	0
094	0	147	0	195	0
097	0	148	0	196	0
098	0	151	0	199	0
103	0	152	0	200	0
104	0	155	0	203	0
107	0	156	0	204	8
108	0	159	0	207	0
111	0	160	0	208	0
112	0	163	0	211	0
115	0	164	5	212	0
116	0	167	0		

Table A2 Error occurrence time by CCTV

CCTV No.	Error occurrence time (yymmdd_hhmmss)	CCTV No.	Error occurrence time (yymmdd_hhmmss)	CCTV No.	Error occurrence time (yymmdd_hhmmss)
047	20201119_080100	071	20201123_110100	164	20201119_030100
062	20201119_100100		20201123_120100		20201119_040100
	20201119_110100		20201123_150100		20201119_050100
	20201119_120100		20201123_170100		20201119_070100
	20201119_130100		20201128_110100		20201119_080100
071	20201118_170100		20201128_160100	183	20201201_080100
	20201119_090100		20201128_170100	204	20201119_010100
	20201119_140100		20201129_170100		20201119_020100
	20201122_170100		20201130_080100		20201119_030100
	20201122_190100		20201130_150100		20201119_040100
	20201122_200100		20201130_170100		20201122_040100
	20201122_210100		20201201_160100		20201122_050100
	20201122_220100		20201201_170100		20201122_060100
	20201122_230100	077	20201119_170100		20201122_070100
	20201123_070100	131	20201129_150100		
	20201123_080100	136	20201120_060100		
	20201123_100100		20201120_070100		

Table A3 Parameters for image preprocessing and circular Hough transformation

CCTV No.	Minimum radius (pixels)	Maximum radius (pixels)	Gamma correction factor	Application of adaptive image binarization
035	21	40	-	○
038	21	40	0.3	○
041	21	40	0.3	○
044	70	100	0.3	×
047	21	50	0.3	○
050	70	100	-	×
053	30	50	0.3	×
056	70	100	0.3	×
059	20	40	0.3	×
062	20	40	0.3	×
065	25	40	0.3	○
068	21	40	0.3	○
071	25	40	-	○
074	20	40	-	×
077	20	40	-	×
093	70	100	-	×
094	70	100	-	×
097	70	90	-	×
098	70	100	-	×
103	70	90	-	×
104	70	100	-	×
107	70	100	-	×
108	70	100	-	×
111	70	100	-	×
112	70	100	-	×
115	70	100	-	×
116	70	100	-	×

Table A3 Continued

CCTV No.	Minimum radius (pixels)	Maximum radius (pixels)	Gamma correction factor	Application of adaptive image binarization
119	70	100	-	×
120	70	100	-	×
123	70	100	-	×
124	70	100	-	×
127	70	100	-	×
128	70	100	-	×
131	70	100	-	×
132	70	100	-	×
135	70	90	-	×
136	70	100	0.3	×
139	70	100	-	×
140	70	100	-	×
143	70	90	-	×
144	70	100	-	×
147	70	100	-	×
148	70	100	-	×
151	70	90	-	×
152	70	100	-	×
155	70	100	-	×
156	70	100	-	×
159	70	90	-	×
160	70	90	-	×
163	70	90	-	×
164	70	90	-	×
167	70	100	-	×
168	70	100	-	×
171	70	100	-	×
172	70	100	-	×
175	70	90	-	×
176	70	100	-	×
179	70	100	-	×
180	70	100	-	×
183	70	100	-	×
184	70	100	-	×
187	60	90	-	×
188	70	100	-	×
191	50	90	-	×
192	70	100	-	×
195	70	100	-	×
196	70	100	-	×
199	70	100	-	×
200	70	100	-	×
203	70	100	-	×
204	70	100	-	×
207	70	100	-	×
208	70	100	-	×
211	70	100	-	×
212	70	100	-	×